Inorg. Chem. **2009**, *48*, 2205−2214

Metal Complexes of a Picolinate-Based Nitronyl Nitroxide Free Radical

Eugenio Coronado, Carlos Giménez-Saiz,‡ Francisco M. Romero,*,‡ and Ana Tarazón

Instituto de Ciencia Molecular, Universitat de València, Polígon La Coma s/n, E-46980 Paterna, Spain

Received November 19, 2008

A nitronyl nitroxide free radical containing an appended picolinate moiety was synthesized. The resulting tridentate ligand picNN forms neutral mononuclear metal complexes of formula $[M(picNN)_2]\cdot 3H_2O$ (M = Mn, Co, Ni, Zn). These compounds are isostructural and crystallize in the orthorhombic *Pnna* space group. The metal complexes have a C_2 symmetric structure, with the metal centers lying on the binary axis and surrounded by two equivalent picNN radicals. The magnetic properties of this family of compounds indicate the presence of very strong metal−radical exchange interactions, ranging from $J_{Ni-rad} = -193$ cm^{-1} to $J_{Mn-rad} = -98$ cm^{-1}. Relatively weak ($J_{rad-rad} = -15$ cm^{-1}) through-space magnetic interactions between free radicals coordinated to the same metal center were also evidenced in the study of the diamagnetic zinc(II) complex. Complexation with Cu^{2+} affords the carboxylate-bridged tetranuclear copper(II) complex $[Cu_4(picNN)_4(H_2O)_4](ClO_4)_4\cdot 4H_2O$ having eight interacting $S = 1/2$ spins in a cyclic topology. The antiferromagnetic copper−radical exchange interaction ($J_{Cu-rad} = -268$ cm^{-1}) is one of the largest ever reported.

Introduction

The synthesis of molecular magnets usually requires the self-assembly of molecular components (*building blocks*) into crystalline extended lattices where magnetic metal ions are connected by bridging ligands that are able to transmit the superexchange interaction.[1] In the so-called "metal−radical approach", the bridging ligand is an open-shell species (organic free radical) bearing an intrinsic magnetic moment that interacts with the metal ions by a direct exchange mechanism.[2,3] Direct interactions are generally stronger and can be easily correlated to structural features.[4,5] Also, by combination of inorganic and organic spin carriers, it is possible to access a wide range of magnetic clusters and networks with different topologies.[6,7] These two facts have propelled a lot of studies on metal−radical complexes over the past 20 years.

Nitronyl nitroxide (NN) free radicals have very poor electron-donating character but are still the most common bridging open-shell units. Their coordination ability is enhanced when the metal center is activated with electron-withdrawing groups, like hexafluoroacetylacetonate ligands. In these cases, some of the coordination positions are blocked, and systems of restrained dimensionality are obtained.[8] Indeed, the first materials to be studied were metal−radical alternating chains that became magnetically ordered at low temperatures.[9,10] More recently, a revival in the study of these systems came from the observation of single-chain magnetic behavior.[11−13] Besides that, attention has been drawn to the design of NN free radicals with

* To whom correspondence should be addressed. Phone: +34 963544405. E-mail: fmrm@uv.es.

‡ Fundació General de la Universitat de València (FGUV).

(1) Kahn, O. *Molecular Magnetism*; VCH: New York, 1993.
(2) Caneschi, A.; Gatteschi, D.; Sessoli, R.; Rey, P. *Acc. Chem. Res.* **1989**, *22*, 392–398.
(3) Caneschi, A.; Gatteschi, D.; Rey, P. *Prog. Inorg. Chem.* **1991**, *39*, 331–429.
(4) Okazawa, A.; Nagaichi, Y.; Nogami, T.; Ishida, T. *Inorg. Chem.* **2008**, *47*, 8859–8868.
(5) Gilroy, J. B.; Koivisto, B. D.; McDonald, R.; Ferguson, M. J.; Hicks, R. G. *J. Mater. Chem.* **2006**, *16*, 2618–2624.
(6) Numata, Y.; Inoue, K.; Baranov, N.; Kurmoo, M.; Kikuchi, K. *J. Am. Chem. Soc.* **2007**, *129*, 9902–9909.
(7) Maspoch, D.; Domingo, N.; Ruiz-Molina, D.; Wurst, K.; Vaughan, G.; Tejada, J.; Rovira, C.; Veciana, J. *Angew. Chem., Int. Ed.* **2004**, *43*, 1828–1832.
(8) Caneschi, A.; Ferraro, F.; Gatteschi, D.; Rey, P.; Sessoli, R. *Inorg. Chem.* **1990**, *29*, 1756–1760.
(9) Caneschi, A.; Gatteschi, D.; Laugier, J.; Rey, P. *J. Am. Chem. Soc.* **1987**, *109*, 2191–2192.
(10) Luneau, D.; Rey, P.; Laugier, J.; Fries, P.; Caneschi, A.; Gatteschi, D.; Sessoli, R. *J. Am. Chem. Soc.* **1991**, *113*, 1245–1251.
(11) Caneschi, A.; Gatteschi, D.; Lalioti, N.; Sangregorio, C.; Sessoli, R.; Venturi, G.; Vindigni, A.; Rettori, A.; Pini, M. G.; Novak, M. A. *Angew. Chem., Int. Ed.* **2001**, *40*, 1760–1763.
(12) Bogani, L.; Sangregorio, C.; Sessoli, R.; Gatteschi, D. *Angew. Chem., Int. Ed.* **2005**, *44*, 5817–5821.
(13) Bernot, K.; Bogani, L.; Caneschi, A.; Gatteschi, D.; Sessoli, R. *J. Am. Chem. Soc.* **2006**, *128*, 7947–7956.

10.1021/ic802218j CCC: $40.75
Published on Web 02/05/2009

chelating properties induced by functionalization with different heterocyclic ligands like pyridine,[14−17] picoline,[18] bipyridine,[19−24] phenanthroline,[20] pyrimidine,[25] triazole,[26] tetrazole,[27] imidazole,[28−31] benzimidazole,[32,33] pyrazole,[34] thiazole,[35] and so forth. Also, podand free radicals bearing aminomethyl subunits were synthesized and sometimes used in the electron paramagnetic resonance detection of alkaline ions.[36−38] Most of these ligands yielded mononuclear metal complexes that have been very useful in the understanding of metal−radical interactions, although magnetic order was not present. The negatively charged bis-chelating imidazole and benzimidazole-based radicals became an interesting exception, as they formed one- and two-dimensional (2D) extended structures with relatively high magnetic ordering temperatures.[39] Another anionic and potentially bis-chelating free radical is the hitherto elusive NN bearing a carboxylate function in the α position.[40] This compound was recently obtained but proved to be too unstable to afford complexation with different metal ions.

Inspired by all of these studies, we have synthesized a tridentate ligand (picNN) derived from the picolinate anion that incorporates a NN unit in the 6- position of the pyridine ring. This chelating free radical contains the chemically stable pyNN moiety and carboxylate anions that modify the charge of the metal complex and can, in principle, act as bridging units in the design of extended structures. We report herein on the syntheses, crystal structures, and magnetic properties of a series of neutral mononuclear metal complexes of the formula $[M(picNN)_2]\cdot 3H_2O$ (M = Ni (**4**), Co (**5**), Zn (**6**), Mn (**7**)) and the carboxylate-bridged tetranuclear copper(II) complex $[Cu_4(picNN)_4(H_2O)_4](ClO_4)_4\cdot 4H_2O$ (**8**).

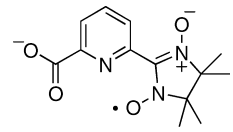

picNN

Experimental Section

Synthesis. 2,3-Bis(hydroxyamino)-2,3-dimethylbutane was prepared as a monosulphate salt according to the Lamchen−Mittag method.[41] Methyl 6-formylpyridine-2-carboxylate was obtained from commercially available dimethyl pyridine-2,6-dicarboxylate by adapting a reported procedure.[42] All other reagents were used as received.

Caution! *Note that perchlorate salts are potentially explosive and should be handled carefully, in low quantities, as hydrated salts.*

Methyl 6-(1,3-Dihydroxy-4,4,5,5-tetramethylimidazolidin-2-yl)pyridine-2-carboxylate (1). The monosulphate salt of 2,3-bis(hydroxyamino)-2,3-dimethylbutane (1.42 g, 5.76 mmol) was dissolved in 50 mL of H_2O, and solid K_2CO_3 (0.8 g, 5.76 mmol) was added to release the free base. Then, methyl 6-formylpyridine-2-carboxylate (0.77 g, 4.6 mmol) was added, and the resulting solution was stirred for 3 h. After a few minutes, the product of condensation precipitated as a white solid that was collected by filtration and dried under vacuum. Yield: 79%. ^{1}H NMR ($CDCl_3$): δ 1.14 (s, 6H; CH_3), 1.20 (s, 6H; CH_3), 3.97 (s, 3H; OCH_3), 5.09 (s, 1H; CH), 5.45 (s, 2H; OH), 7.79 (d, H_A; J_{AB} = 7.9 Hz, J_{AC} = 0.9 Hz), 7.84 (t, H_B; J_{BC} = 7.7 Hz), 8.05 (d, H_B). ES-MS (CH_3OH): 317.86 $[M + Na^+]^+$. IR (KBr, cm^{-1}): 3514 (NO−H), 1709 (C═O), 1368 (N−O), 1141 (N−O). Elem anal. calcd for $C_{14}H_{21}N_3O_4\cdot 1.5H_2O$: C, 52.16; H, 7.50; N, 13.04. Found: C, 51.86; H, 6.77; N, 12.82.

Methyl 6-(1-Oxyl-3-oxide-4,4,5,5-tetramethylimidazolin-2-yl)pyridine-2-carboxylate (2). The radical precursor **1** (1.07 g, 3.62 mmol) was suspended in 200 mL of CH_2Cl_2. Then, a solution of $NaIO_4$ (0.77 g, 3.59 mmol) in 200 mL of H_2O was added, and the resulting biphasic mixture was stirred for 45 min. The organic phase was separated, washed with water, and dried over $MgSO_4$. Evaporation of the solvent afforded a violet oily residue that precipitated after the addition of pentane. Recrystallization from a dichloromethane−hexane mixture yielded the free radical as violet crystals. Yield: 60%. ES-MS (CH_3CN): 314.77 $[M + Na^+]^+$, 292.84 $[M + H^+]^+$. IR (KBr, cm^{-1}): 1720 (C═O), 1371 (N−O), 1130 (N−O). Elem anal. calcd for $C_{14}H_{18}N_3O_4$: C, 57.52; H, 6.21; N, 14.38. Found: C, 57.39; H, 6.26; N, 14.35.

(14) Luneau, D.; Risoan, G.; Rey, P.; Grand, A.; Caneschi, A.; Gatteschi, D.; Laugier, J. *Inorg. Chem.* **1993**, *32*, 5616–5622.
(15) Francese, G.; Romero, F. M.; Neels, A.; Stoeckli-Evans, H.; Decurtins, S. *Inorg. Chem.* **2000**, *39*, 2087–2095.
(16) Oshio, H.; Yamamoto, M.; Ito, T.; Kawauchi, H.; Koga, N.; Ikoma, T.; Tero-Kubota, S. *Inorg. Chem.* **2001**, *40*, 5518–5525.
(17) Li, L.; Liao, D.; Jiang, Z.; Mouesca, J.-M.; Rey, P. *Inorg. Chem.* **2006**, *45*, 7665–7670.
(18) Yamamoto, Y.; Suzuki, T.; Kaizaki, S. *J. Chem. Soc., Dalton Trans.* **2001**, 2943–2950.
(19) Ulrich, G.; Ziessel, R.; Luneau, D.; Rey, P. *Tetrahedron Lett.* **1994**, *35*, 1211–1214.
(20) Luneau, D.; Laugier, J.; Rey, P.; Ulrich, G.; Ziessel, R.; Legoll, P.; Drillon, M. *J. Chem. Soc., Chem. Commun.* **1994**, 741–742.
(21) Romero, F. M.; Luneau, D.; Ziessel, R. *Chem. Commun.* **1998**, 551–552.
(22) Luneau, D.; Romero, F. M.; Ziessel, R. *Inorg. Chem.* **1998**, *37*, 5078–5087.
(23) Luneau, D.; Stroh, C.; Cano, J.; Ziessel, R. *Inorg. Chem.* **2005**, *44*, 633–637.
(24) Ziessel, R.; Ulrich, G.; Lawson, R. C.; Echegoyen, L. *J. Mater. Chem.* **1999**, *9*, 1435–1448.
(25) Omata, J.; Ishida, T.; Hashizume, D.; Iwasaki, F.; Nogami, T. *Inorg. Chem.* **2001**, *40*, 3954–3958.
(26) Kahn, M. L.; Sutter, J.-P.; Golhen, S.; Guionneau, P.; Ouahab, L.; Kahn, O.; Chasseau, D. *J. Am. Chem. Soc.* **2000**, *122*, 3413–3421.
(27) Tretyakov, E. V.; Fokin, S. V.; Romanenko, G. V.; Ovcharenko, V. I. *Polyhedron* **2003**, *22*, 1965–1972.
(28) Fegy, K.; Sanz, N.; Luneau, D.; Belorizky, E.; Rey, P. *Inorg. Chem.* **1998**, *37*, 4518–4523.
(29) Fegy, K.; Luneau, D.; Belorizky, E.; Novac, M.; Tholence, J.-L.; Paulsen, C.; Ohm, T.; Rey, P. *Inorg. Chem.* **1998**, *37*, 4524–4532.
(30) Fegy, K.; Luneau, D.; Ohm, T.; Paulsen, C.; Rey, P. *Angew. Chem Int. Ed.* **1998**, *37*, 1270–1273.
(31) Aoki, C.; Ishida, T.; Nogami, T. *Inorg. Chem.* **2003**, *42*, 7616–7625.
(32) Lescop, C.; Belorizky, E.; Luneau, D.; Rey, P. *Inorg. Chem.* **2002**, *41*, 3375–3384.
(33) Lescop, C.; Luneau, D.; Rey, P.; Bussière, G.; Reber, C. *Inorg. Chem.* **2002**, *41*, 5566–5574.
(34) Yamada, S.; Yasui, M.; Nogami, T.; Ishida, T. *Dalton Trans.* **2006**, 1622–1626.
(35) Lin, H.-H.; Mohanta, S.; Lee, C.-J.; Wei, H.-H. *Inorg. Chem.* **2003**, *42*, 1584–1589.
(36) Ulrich, G.; Turek, P.; Ziessel, R. *Tetrahedron Lett.* **1996**, *37*, 8755–8758.
(37) Ulrich, G.; Turek, P.; Ziessel, R.; De Cian, A.; Fischer, J. *Chem. Commun.* **1996**, 2461–2462.
(38) Vostrikova, K. E.; Belorizky, E.; Pécaut, J.; Rey, P. *Eur. J. Inorg. Chem.* **1999**, 1181–1187.
(39) Luneau, D.; Rey, P. *Coord. Chem. Rev.* **2005**, *249*, 2591–2611.
(40) Tretyakov, E.; Fokin, S.; Ovcharenko, V.; Romanenko, G.; Shvedenkov, Y. *Polyhedron* **2005**, *24*, 2176–2184.
(41) Lamchen, M.; Mittag, T. W. *J. Chem. Soc. C* **1966**, 2300–2303.
(42) Platas-Iglesias, C.; Mato-Iglesias, M.; Djanashvili, K.; Muller, R. N.; Van der Elst, L.; Peters, J. A.; de Blas, A.; Rodríguez-Blas, T. *Chem.—Eur. J.* **2004**, *10*, 3579–3590.

Table 1. X-Ray Crystallographic Data for **4**−**8**

	4	**5**	**6**	**7**	**8**
chemical formula	$C_{26}H_{36}N_6NiO_{11}$	$C_{26}H_{36}CoN_6O_{11}$	$C_{26}H_{36}N_6O_{11}Zn$	$C_{26}H_{36}MnN_6O_{11}$	$C_{52}H_{76}Cl_4Cu_4N_{12}O_{40}$
a (Å)	7.51620(10)	7.56670(10)	7.53970(10)	7.52800(10)	19.4360(2)
b (Å)	27.7143(4)	27.8458(6)	27.9622(4)	28.0110(5)	10.5109(2)
c (Å)	13.7502(2)	13.8927(2)	13.9281(2)	14.0710(2)	21.6980(3)
α (deg)	90	90	90	90	90
β (deg)	90	90	90	90	123.804(2)
γ (deg)	90	90	90	90	90
V (Å^3)	2864.25(7)	2927.20(9)	2936.41(7)	2967.11(8)	3683.32(13)
T (K)	180(2)	293(2)	293(2)	293(2)	180(2)
Z	4	4	4	4	2
fw	667.32	667.54	673.98	663.55	1905.21
cryst syst	orthorhombic	orthorhombic	orthorhombic	orthorhombic	monoclinic
space group	*Pnna*	*Pnna*	*Pnna*	*Pnna*	$P2_1/c$
ρ_{calcd} (g·cm^{-3})	1.548	1.515	1.525	1.485	1.718
μ (mm^{-1})	0.749	0.657	0.907	0.515	1.391
$R(F_o)$, $Rw(F_o^2)$ $[I < 2\sigma(I)]^a$	0.0372, 0.0829	0.0397, 0.0838	0.0417, 0.1087	0.0430, 0.1090	0.0417, 0.0980

^{a} $R = \sum(F_o - F_c)/\sum F_o$; $R_w = \{\sum[w(F_o^2 - F_c^2)^2]/\sum[w(F_o^2)^2]\}^{1/2}$.

Lithium 6-(1-Oxyl-3-oxide-4,4,5,5-tetramethylimidazolin-2-yl)pyridine-2-carboxylate (3). The methyl ester **2** (0.63 g, 2.15 mmol) was dissolved in 20 mL of THF. An aqueous solution (20 mL) of LiOH (0.051 g, 2.15 mmol) was added, and the resulting mixture was stirred for 30 min. The solvents were evaporated, and the blue residue was recrystallized from a dichloromethane−ethyl acetate mixture to afford blue needles of **3**. Yield: 49%. ES-MS (CH_3CN): 277.87 $[M - Li^+ + H^+ - 1e^-]^+$, 284.87 $[M + H^+]^+$. IR (KBr, cm^{-1}): 3414 (O−H), 1737 (C═O), 1361 (N−O), 1178 (N−O). UV−vis (CH_3CN), λ (nm; ε (M^{-1}·cm^{-1})): 362 (18 400), 577 (390). Elem anal. calcd for $C_{13}H_{15}LiN_3O_4 \cdot 2.5H_2O$: C, 47.42; H, 6.12; N, 12.76. Found: C, 47.38; H, 6.15; N, 12.11.

Metal Complexes 4−7. A total of 100 mg (0.35 mmol) of the lithium salt **3** was dissolved in 2 mL of EtOH. Then, a solution of $M(ClO_4)_2 \cdot 6H_2O$ (140 mg, 0.38 mmol) in 2 mL of EtOH was added. After the two solutions were mixed, two drops of water were added, and the resulting mixture was allowed to stand at room temperature. Single crystals suitable for X-ray structure determination were obtained in a few days.

$[Ni(picNN)_2]\cdot 3H_2O$ (4). IR (KBr, cm^{-1}): 1683 (C═O), 1359 (N−O), 1122 (N−O). Elem anal. calcd for $C_{26}H_{36}N_6NiO_{11}$: C, 46.80; H, 5.44; N, 12.59. Found: C, 46.25; H, 5.40; N, 12.28.

$[Co(picNN)_2]\cdot 3H_2O$ (5). IR (KBr, cm^{-1}): 1653 (C═O), 1350 (N−O), 1122 (N−O). Elem anal. calcd for $C_{26}H_{36}CoN_6O_{11}$: C, 46.78; H, 5.44; N, 12.59. Found: C, 46.50; H, 5.35; N, 12.10.

$[Zn(picNN)_2]\cdot 3H_2O$ (6). IR (KBr, cm^{-1}): 1652 (C═O), 1348 (N−O), 1183 (N−O). Elem anal. calcd for $C_{26}H_{36}N_6O_{11}Zn$: C, 46.33; H, 5.38; N, 12.47. Found: C, 46.15; H, 5.55; N, 12.20.

$[Mn(picNN)_2]\cdot 3H_2O$ (7). IR (KBr, cm^{-1}): 1650 (C═O), 1350 (N−O), 1180 (N−O). Elem anal. calcd for $C_{26}H_{36}MnN_6O_{11}$: C, 47.06; H, 5.47; N, 12.67. Found: C, 46.93; H, 5.58; N, 12.64.

$[Cu_4(picNN)_4(H_2O)_4](ClO_4)_4\cdot 4H_2O$ (8). IR (KBr, cm^{-1}): 1637 (C═O), 1375 (N−O), 1121 (Cl−O). Elem anal. calcd for $C_{52}H_{60}Cl_4Cu_4N_{12}O_{32}$: C, 35.46; H, 3.43; N, 9.54. Found: C, 36.11; H, 3.48; N, 9.49.

Crystal Structure Determination. The crystal structures of compounds **4**−**8** were determined from single-crystal X-ray diffraction data collected at 180(2) K for **4** and **8** and at 293(2) K for **5**, **6**, and **7**. Compounds **4**−**7** were found to be isostructural. Data were collected with a Nonius KappaCCD diffractometer using a graphite monochromated Mo Kα radiation source (λ = 0.71073 Å). The Denzo and Scalepack[43] programs were used for cell refinements and data reduction. The structures were solved by direct methods using the SIR97[44] program with the WinGX graphical user interface.[45] The structure refinements were carried out with SHELX-97.[46] No absorption corrections were performed. All non-hydrogen atoms were refined anisotropically. Hydrogen atoms on carbon atoms were included at calculated positions and refined with a riding model. The H atoms of water molecules were all found in difference maps and refined positionally with geometric restraints (O−H = 0.82 Å and H···H = 1.30 Å) and with $U_{iso}(H) = 1.2U_{eq}(O)$. Crystal data are gathered in Table 1.

Physical Techniques. The dc magnetic susceptibility measurements were performed on polycrystalline samples using a magnetometer (Quantum Design MPMS-XL-5) equipped with a SQUID sensor. Variable-temperature measurements were carried out in the temperature range 2−400 K in a magnetic field of 0.1 T. In the analysis of the magnetic properties of **4**−**7**, the total Hamiltonian of the system was solved for different values of relevant parameters using the MAGPACK code.[47]

^{1}H NMR spectra were recorded on a Bruker Avance DRX-300 spectrometer at room temperature using deuterated chloroform as an internal standard.

Electrospray ionization mass spectra (positive mode) were recorded on a Waters ZQ mass spectrometer using nitrogen as a drying and nebulizing gas. The cone voltage was set to 50 V.

Optical absorption spectra were recorded on an Agilent 8453 spectrophotometer in the 200−800 nm wavelength range.

IR transmission measurements of KBr pellets were recorded at room temperature with a Nicolet Avatar 320 FT-IR spectrophotometer in the range 4000−400 cm^{-1}.

CHN elemental analyses were carried out on a CE instruments EA 1110 CHNS analyzer.

Results and Discussion

Synthesis. All of the complexes described in this work were obtained by direct complexation of picNN to the corresponding metal perchlorate salts. The anionic ligand picNN (Scheme 1) was obtained as a lithium salt by saponification of the methyl ester **2**, which was synthesized

(43) Otwinowski, Z.; Minor, W. DENZO-SCALEPACK, Processing of X-ray Diffraction Data Collected in Oscillation Mode. In *Methods in Enzymology*; Carter, C. W., Jr., Sweet, R. M., Eds.; Academic Press: New York, 1997; Vol. 276, Macromolecular Crystallography, Part A.
(44) Altomare, A.; Burla, M. C.; Camalli, M.; Cascarano, G.; Giacovazzo, C.; Guagliardi, A.; Moliterni, A. G. G.; Polidori, G.; Spagna, R. *J. Appl. Crystallogr.* **1999**, *32*, 115–119.
(45) Farrugia, L. J. *J. Appl. Crystallogr.* **1999**, *32*, 837–838.
(46) Sheldrick, G. M. *SHELXL-97*; University of Göttingen: Göttingen, Germany, 1997.
(47) Borrás-Almenar, J. J.; Clemente-Juan, J. M.; Coronado, E.; Tsukerblat, B. S. *J. Comput. Chem.* **2001**, *22*, 985–991.

Scheme 1[a]

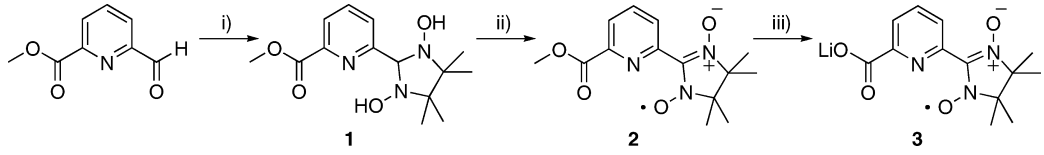

[a] (i) 2,3-Bis(hydroxyamino)-2,3-dimethyl butane monosulphate salt, K_2CO_3, H_2O; (ii) $NaIO_4$, CH_2Cl_2/H_2O; (iii) LiOH, THF/H_2O.

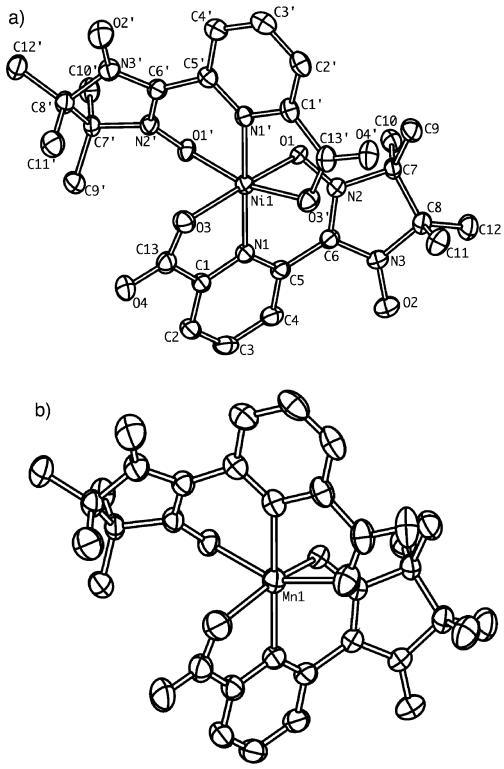

Figure 1. Thermal ellipsoid plots of **4** and **7** showing the atom numbering scheme. Symmetry code: N1′ = N1(x, $-y + 1/2$, $-z + 1/2$).

from methyl 6-formylpyridine-2-carboxylate following the Ullman procedure.[48]

Crystal Structures of $[M(picNN)_2]\cdot 3H_2O$ [M = Ni (4), Co (5), Zn (6), Mn (7)]. Compounds **4**−**7** are isostructural and crystallize in the orthorhombic *Pnna* space group. The four compounds crystallize as hydrates that contain three water molecules per formula unit. In all of the structures, radical picNN behaves as a tridentate ligand, with one N(pyridine) atom, one O(aminoxyl) atom, and one O(carboxylate) atom occupying meridional positions of a distorted octahedron (Figure 1). The torsion angle between the two heterocyclic fragments inside the picNN anion lies in a small range around 30°. The bond distances of the coordinated nitroxide fragments (mean value: 1.295 ± 0.004 Å) are significantly higher than those corresponding to the free N−O units (mean value: 1.267 ± 0.005 Å). These features were commonly observed in other chelating NN compounds.[14−17] The metal center lies on a binary axis and is surrounded by two equivalent picNN ligands. The free radical subunits occupy two cis positions of the N_2O_4 coordination sphere, while the pyridine rings are located in a trans arrangement.

(48) Ullman, E. F.; Osiecki, J. H.; Boocock, D. G. B.; Darcy, R. *J. Am. Chem. Soc.* **1972**, *94*, 7049–7059.

Table 2. Selected intramolecular dihedral angles for **4**−**7**

dihedral angle[a]	Ni (**4**)	Co (**5**)	Zn (**6**)	Mn (**7**)
basal plane, rad	75.12(10)°	74.11(13)°	73.21(14)°	72.83(11)°
xz (yz) plane, rad	51.27(12)°	51.60(15)°	52.09(16)°	50.31(12)°
rad, rad	33.01(10)°	35.35(13)°	37.26(14)°	36.66(10)°

[a] Least-squares mean planes have been defined as follows: basal plane ($x^2 - y^2$) = O1−O3−M−O3′−O1′, xz (yz) plane = N1−O1−M−O3−N1′, rad = O1−N2−C6−N3-O2. Symmetry code: N1′ = N1(x, $-y + 1/2$, $-z + 1/2$).

In the following, the mean plane formed by the four O donors will be considered the basal plane of the complex. The pyridine rings occupy then the axial positions. In the establishment of magneto-structural correlations in metal−radical complexes, it has been shown that the relevant structural features are the dihedral angles between planes located parallel or perpendicular to the direction of magnetic orbitals.[15,22] These values are listed in Table 2 for complexes **4**−**7**.

The nickel(II) complex **4** shows the least distorted octahedral arrangement (Figure 1a). The Ni−N1 (2.0169(17) Å) and Ni−O3 (2.0315(14) Å) bond lengths are similar, the free radical being located at a slightly greater distance (Ni−O1 = 2.0842(14) Å). In contrast with previously reported tridentate radical ligands,[15] the basal plane shows a severe distortion, with bond angles that depart considerably from 90° (for instance, O3−Ni−O3′ = 102.62(9)° and O1−Ni−O1′ = 85.02(8)°). This is a consequence of the different bite angles for the picolinate and pyNN chelating fragments. Outside the basal plane, the N1−Ni−O3 bond angles (97.75(6)° and 81.76(6)°) show the largest deviation from octahedral geometry. The high degree of distortion brings the two carboxylate O3 atoms to be located 0.1739(9) Å above and below the mean equatorial plane, while the two nitroxide O1 atoms sit even at a higher distance (±0.197(1) Å).

The analogous cobalt(II) and zinc(II) complexes **5** and **6** show very similar coordination spheres. The metal−carboxylate distances, mainly governed by electrostatic interactions, are practically the same in the three compounds (Co−O3, 2.0396(18) Å for **5**; Zn−O3, 2.035(2) Å for **6**). Instead, the more covalent metal−pyridine and metal−radical bond distances increase considerably on going from **4** to **6** (Co−N1, 2.068(2) Å and Co−O1, 2.1240(16) Å for **5**; Zn−N1, 2.085(2) Å and Zn−O1, 2.2081 (19) Å for **6**). As the size of the metal ion increases, the distortion of the coordination sphere in the equatorial plane becomes higher (O3−Co−O3′ = 106.88(11)° and O1−Co−O1′ = 83.24(9)° for **5**; O3−Zn−O3′ = 109.55(13)° and O1−Zn−O1′ = 81.35(10)° for **6**). Increasing deviations from the ideal

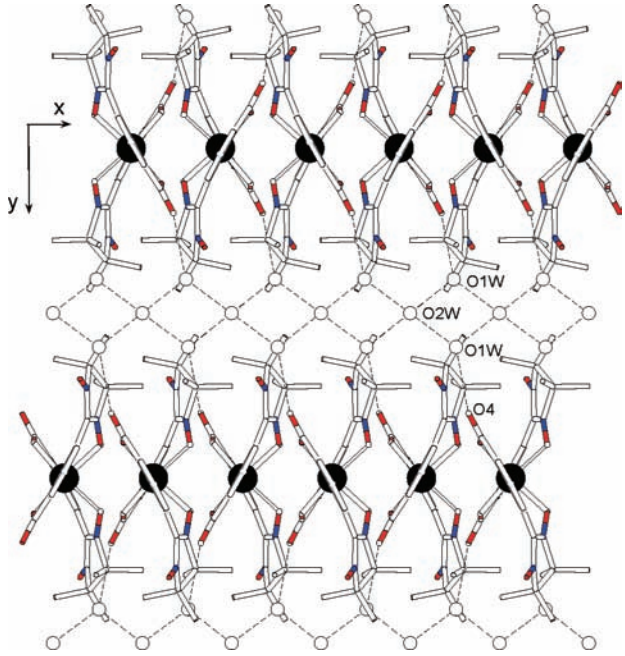

Figure 2. Projection of the crystal structure of **4** onto the *ab* plane. Dashed lines refer to hydrogen bonds. Black circles represent Ni atoms. Blue and red cylinders refer to N and O atoms, respectively.

geometry are also observed outside the basal plane (N1−M−O3 bond angles, 99.30(8)° and 80.56(8)° for **5** and 101.52(9)° and 80.76(9)° for **6**).

The isostructural manganese(II) compound **7** exhibits a slightly different coordination environment (Figure 1b). Here, the metal−pyridine bond distance (Mn−N1, 2.2139(18) Å) is higher than the metal−oxygen distances found in the basal plane (Mn−O1, 2.1760(14) Å; Mn−O3, 2.1046(16) Å). The bigger size of the central Mn^{2+} ion imposes the highest geometrical distortion in these series, mostly along the axial direction, with N1−Mn−O3 bond angles of 103.84(6)° and 76.29(6)°. The distance from the mean equatorial plane to the positions of the two nitroxide O1 atoms is longer than 0.44 Å.

The crystal packing of compounds **4**−**7** is shown in Figure 2. The neutral metal−radical complexes form layers that run perpendicular to the *b* axis. The free oxygen atoms from the carboxylate units (O4) point outside the layers and are hydrogen-bonded to water molecules (O4−O1W: 2.848(2) Å (**4**), 2.873(3) Å (**5**), 2.880(3) Å (**6**), 2.893(3) Å (**7**)). The remaining water molecules, O2W, lie on a binary axis and are hydrogen-bonded to O1W, connecting the layers along the *b* axis. Inside the layers, the metal−radical complexes form stacks parallel to the *a* axis (Figure 3) due to the presence of strong $\pi-\pi$ interactions between adjacent pyridine rings. This situation induces a short intermolecular contact between two free nitroxide groups (O2−O2(x + 1/2, y, 1 − z): 3.759(2) Å (**4**), 3.783(2) Å (**5**), 3.770(2) Å (**6**), 3.764(2) Å (**7**)) that propagates to form chains of radicals running along the *x* direction.

Crystal Structure of $[Cu_4(picNN)_4(H_2O)_4](ClO_4)_4\cdot 4H_2O$ (8). The copper(II) compound **8** crystallizes in the monoclinic $P2_1/c$ space group. The structure of the tetranuclear complex (Figure 4) is centrosymmetric and contains two inequivalent

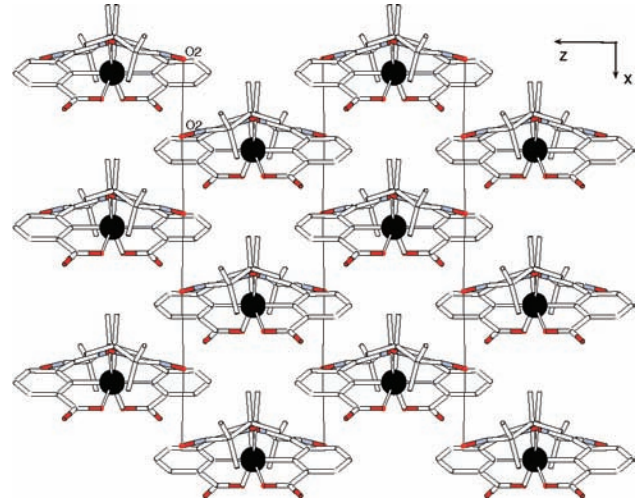

Figure 3. Projection of the crystal structure of **4** onto the *ac* plane. Thin lines represent the shortest contacts between nitroxides. Black circles represent Ni atoms. Blue and red cylinders refer to N and O atoms, respectively.

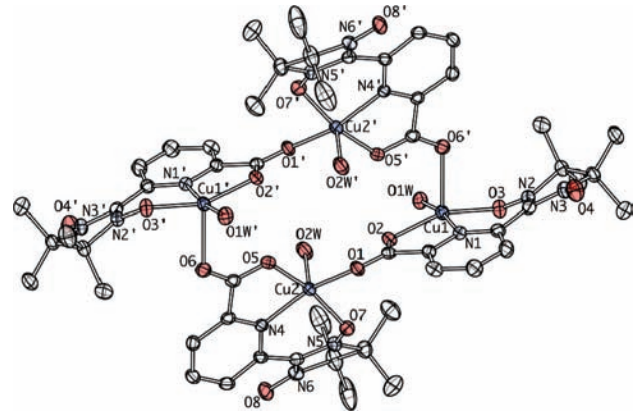

Figure 4. Thermal ellipsoid plot of a tetrameric unit of **8** showing the atom numbering. Symmetry code: N1′ = N1(−x + 1, −y, −z).

picNN ligands and two Cu^{2+} ions (denoted as Cu1 and Cu2) in a slightly distorted square-pyramidal geometry. The basal plane of Cu1 is occupied by one tridentate radical (picNN) and one water molecule. The shortest metal−ligand bond distance for this metal center corresponds to the copper(II)−nitroxide bond (Cu1−O3 = 1.9387(19) Å). The remaining bond distances in the basal plane are shorter than 2 Å, as expected for a copper(II) complex (Cu1−O1W = 1.940(2) Å; Cu1−O2 = 1.9591(19) Å; Cu1−N1 = 1.971(2) Å). The radical ligand picNN connects the two copper(II) sites through their basal positions by a syn−anti carboxylate bridge (Cu2−O1 = 1.9571(19) Å). A second picNN molecule occupies the remaining positions in the Cu2 basal plane. Again, the shortest metal−ligand bond distance corresponds to the copper(II)−nitroxide bond (Cu2−O7 = 1.9444(19) Å; Cu2−O5 = 1.9487(19) Å; Cu2−N4 = 1.981(2) Å). A water molecule is found in the apical position of the Cu2 coordination sphere (Cu2−O2W = 2.208(2) Å). Finally, the dicopper(II) units are connected through the apical position of Cu1 by another syn−anti carboxylate bridge (Cu1−O6′ = 2.2507(19) Å) to yield the tetrameric ring. The four metal sites define a parallelogram with a Cu2−Cu1−Cu2 angle of 64.64(1)°. The distance between

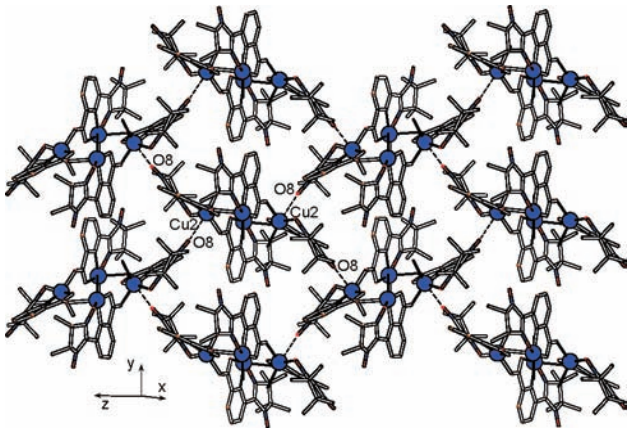

Figure 5. View of the crystal structure of **8** showing the connection of $[Cu_4(picNN)_4(H_2O)_4]^{4+}$ units by weak copper−nitroxide bonding.

Cu^{2+} ions linked through their basal positions is 5.0656(5) Å, significantly shorter than the separation between copper ions related by an equatorial−axial syn−anti carboxylate bridge (Cu1−Cu2 = 5.1314(5) Å).

The torsion angle between the two heterocyclic fragments inside the first picNN anion (21.6(3)°) is very small as compared to other chelating NN compounds. The bond distances of the coordinated nitroxide fragments (mean value: 1.3025 ± 0.0015 Å) are significantly longer than those measured for complexes **4**−**7**. These two features are indicative of very strong copper−radical electronic interactions. The dihedral angles between the mean basal planes of the carboxylate-bridged copper(II) sites are very similar and close to 68°. In the study of the magnetic properties of copper(II)−radical complexes, the crucial structural feature to be discussed is the dihedral angle between the equatorial plane of the metal and the mean O−N−C−N−O plane of the radical, where most of the spin density is located. The values of these angles for Cu1−NN and Cu2−NN fragments are 22.2(3)° and 33.3(2)°, respectively.

A very weak axial interaction between Cu1 and one perchlorate anion is found (Cu1−O15 = 3.431(4) Å). Also, one of the free nitroxide moieties is weakly coordinated to Cu2 in the axial position (Cu2−O8($-x + 1$, $y + 1/2$, $-z + 1/2$) = 3.098(2) Å, dashed bonds in Figure 5). This contact organizes the tetranuclear copper(II) complexes in a two-dimensional squarelike lattice. The layers are parallel to the *bc* plane and pack themselves along the *a* axis by an intrincate hydrogen-bonded network (Figure 6) that involves the coordinated water molecules, the perchlorate anions, and water of crystallization.

Magnetic Properties. $[Ni(picNN)_2]\cdot 3H_2O$ (4). At room temperature, the product of molar magnetic susceptibility and temperature (χT = 0.40 emu·K·mol^{-1}) is much smaller (Figure 7) than the calculated value (χT = 1.85 emu·K·mol^{-1}) for the sum of the paramagnetic contributions of one nickel(II) center ($S = 1$, $g = 2.1$) and two nitroxide radicals ($S = 1/2$, $g = 2.0$). On decreasing the temperature, χT decreases monotonically and practically vanishes below 100 K, indicating a diamagnetic $S = 0$ ground state that results from antiferromagnetic coupling between the Ni^{2+} ion and the two free radicals. For a quantitative analysis of

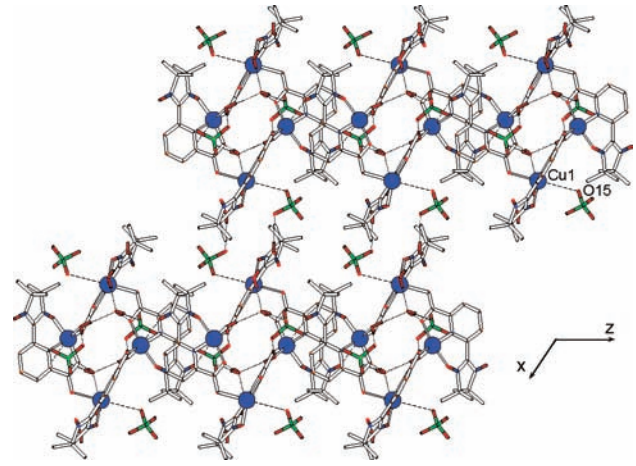

Figure 6. Projection of the crystal structure of **8** onto the *ac* plane showing the arrangement of perchlorate anions in the lattice.

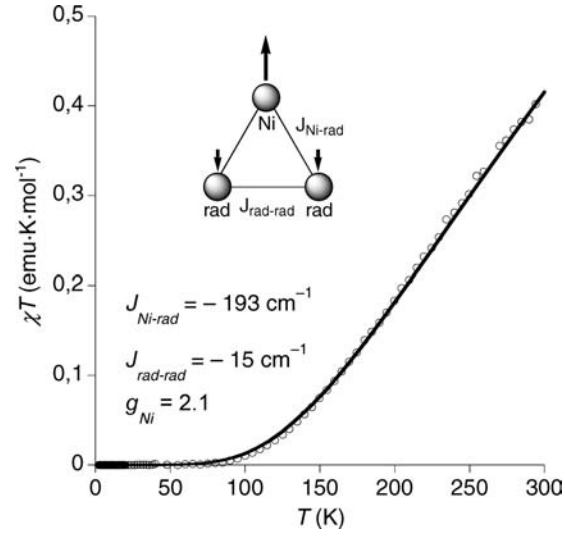

Figure 7. Temperature dependence of the χT product of **4** (empty circles) and best simulation using the exchange Hamiltonian of eq 1. Inset: Exchange interaction pattern and values of the calculated parameters.

the magnetic interactions present in the system (see the pattern depicted in Figure 7), the following isotropic exchange Hamiltonian has been used:

$$\mathbf{H} = -2J_{Ni-rad}(\mathbf{S}_{Ni}\mathbf{S}_{rad1} + \mathbf{S}_{Ni}\mathbf{S}_{rad2}) - 2J_{rad-rad}(\mathbf{S}_{rad1}\mathbf{S}_{rad2}) \quad (1)$$

Equation 1 takes into account that the two radicals are equivalent and considers a radical−radical through-space exchange interaction related to the parameter $J_{rad-rad}$. This interaction is evidenced in the study of the isostructural zinc(II) complex (see below) and has been kept constant for the whole series of complexes. The best-fit data were obtained with the following parameters: $J_{Ni-rad} = -193$ cm^{-1}, $J_{rad-rad} = -15$ cm^{-1}, and $g_{Ni} = 2.1$.

$[Co(picNN)_2]\cdot 3H_2O$ (5). The value of χT at 300 K (1.60 emu·K·mol^{-1}) is well below (Figure 8) the calculated "spin-only" value for one $S = 3/2$ and two $S = 1/2$ spins in the absence of magnetic interactions (2.625 emu·K·mol^{-1}). Taking into account the orbital contribution of the Co^{2+} ion, a limiting high-temperature value around 3.1 emu·K·mol^{-1} should be really observed for a completely uncorrelated

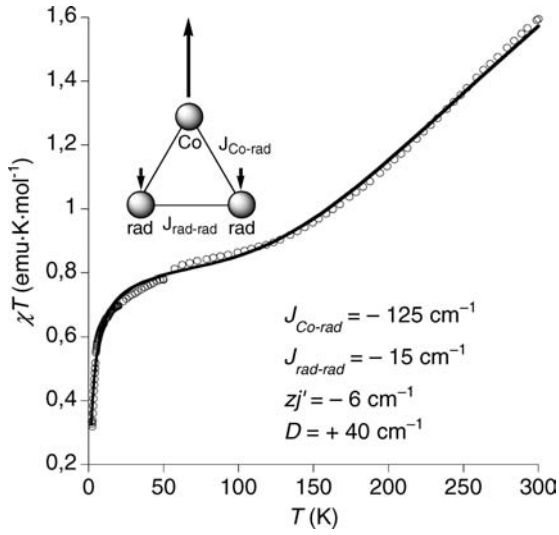

Figure 8. Temperature dependence of the χT product of **5** (empty circles) and best simulation using the full Hamiltonian of eq 2. Inset: Exchange interaction pattern and values of the calculated parameters.

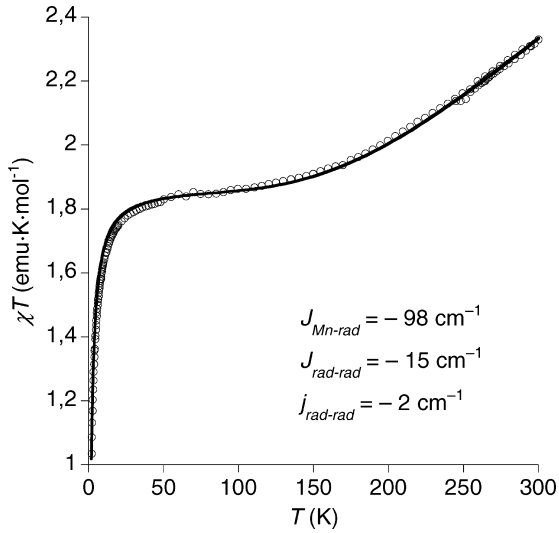

Figure 9. Temperature dependence of the χT product of **7** (empty circles) and best simulation using the exchange Hamiltonian of eq 3. Inset: Values of the calculated parameters. The exchange interaction pattern is shown in Scheme 2.

system. Upon lowering the temperature, χT decreases continuously and tends toward a value around 0.8 emu·K·mol^{-1} at 50 K. Further cooling yields an abrupt decrease of χT to reach 0.33 emu·K·mol^{-1} at the lowest temperature of the experiment (2 K).

The magnetic measurements point clearly to the presence of very strong antiferromagnetic interactions between the cobaltous ion and the nitroxide free radicals. In the low-temperature limit, an effective $S = 1/2$ ground state (with $g > 2$) results from the coupling between the Co(II) Kramers doublet and the two equivalent $S = 1/2$ nitroxide spins. In the quantitative analysis of the magnetic data, we have considered a strong-field electronic configuration for the Co^{2+} ion. In this environment, only the two lowest Kramers doublets arising from the $^4A_{2g}$ ground state are thermally populated. The energy separation D between

Scheme 2

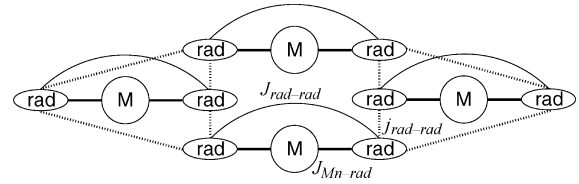

the two doublets can be treated as a zero-field splitting within the $S = 3/2$ state. The full Hamiltonian of the system is then given by the sum of exchange, zero-field splitting, and Zeeman terms (eq 2). The exchange term is expressed now as the addition of intramolecular (metal−radical and radical−radical) interactions and intermolecular interactions. The latter were considered in the frame of the mean-field approximation.

$$\mathbf{H} = -2J_{\mathrm{Co-rad}}(\mathbf{S}_{\mathrm{Co}}\mathbf{S}_{\mathrm{rad1}} + \mathbf{S}_{\mathrm{Co}}\mathbf{S}_{\mathrm{rad2}}) - 2J_{\mathrm{rad-rad}}(\mathbf{S}_{\mathrm{rad1}}\mathbf{S}_{\mathrm{rad2}}) - zj'\sum_i \langle S_z\rangle_i \mathbf{S}_i + D(S_z^2 - 5/4) + \sum_i \beta \mathbf{S}_i \mathbf{g} H \quad (2)$$

The best fit afforded the following values for the different parameters: $J_{\mathrm{Co-rad}} = -125$ cm^{-1}, $J_{\mathrm{rad-rad}} = -15$ cm^{-1}, $zj' = -6$ cm^{-1}, $D = +40$ cm^{-1}, $g_{\|} = 3.00$, $g_{\perp} = 2.37$.

[Mn(picNN)$_2$]·3H$_2$O (7). The χT product at 300 K (2.33 emu·K·mol^{-1}) is far below (Figure 9) the expected value (5.125 emu·K·mol^{-1}) for a noninteracting spin system containing one Mn^{2+} cation ($S = 5/2$) and two nitroxide radicals ($S = 1/2$). Upon cooling, χT decreases continuously and tends toward a plateau with a value of 1.85 emu·K·mol^{-1}, as expected for an $S = 3/2$ ground state. Below 50 K, χT decreases more abruptly to reach a value of 1.04 emu·K·mol^{-1} at the lowest temperature of the experiment (1.98 K). This decrease points to the presence of weak intermolecular interactions.

The $S = 3/2$ ground state results from antiferromagnetic coupling between the Mn^{2+} cation and the two nitroxide radicals located in its coordination sphere. A quantitative analysis of the magnetic properties of **7** was carried out after diagonalization of the exchange Hamiltonian expressed by eq 3, which takes into account the metal−radical interaction $J_{\mathrm{M-rad}}$, the radical−radical interaction within the same complex $J_{\mathrm{rad-rad}}$, and an intermolecular interaction between free radicals $j_{\mathrm{rad-rad}}$. Each radical interacts with two neighboring nitroxides in a regular chain (Figure 3) in such a way that each Mn(picNN)$_2$ unit couples to four adjacent complexes to form a two-dimensional lattice. For the simulation of the magnetic properties of **7**, the 2D system has been modeled by a closed coupled cluster that comprises only four Mn(picNN)$_2$ units, as shown in Scheme 2. The best-fit data yielded the following parameters: $J_{\mathrm{Mn-rad}} = -98$ cm^{-1}, $J_{\mathrm{rad-rad}} = -15$ cm^{-1}, and $j_{\mathrm{rad-rad}} = -2$ cm^{-1}. The value of $j_{\mathrm{rad-rad}}$ has been used as a first estimation of the intermolecular interaction in the zinc(II) complex.

$$\mathbf{H} = -2J_{\mathrm{M-rad}} \sum_{i=1}^{4} (\mathbf{S}_{\mathrm{M}}\mathbf{S}_{\mathrm{rad1}} + \mathbf{S}_{\mathrm{M}}\mathbf{S}_{\mathrm{rad2}})_i - 2J_{\mathrm{rad-rad}} \sum_{i=1}^{4} (\mathbf{S}_{\mathrm{rad1}}\mathbf{S}_{\mathrm{rad2}})_i - 2j_{\mathrm{rad-rad}} \sum_{i=1}^{4} \sum_{j=3}^{4} (\mathbf{S}_{\mathrm{rad1}} + \mathbf{S}_{\mathrm{rad2}})_i (\mathbf{S}_{\mathrm{rad}i})_j \quad (3)$$

[Zn(picNN)$_2$]·3H$_2$O (6). The value of the χT product (Figure 10a) at room temperature (0.72 emu·K·mol^{-1}) is slightly lower than the expected value for two uncorrelated radical $S = 1/2$ spins (0.75 emu·K·mol^{-1}). As the sample is cooled, χT decreases smoothly. Below 50 K, the decrease is more pronounced, and the χT product tends to zero at the lowest temperature of the experiment. The thermal variation of the molar magnetic susceptibility χ exhibits (Figure 10b) a maximum at $T = 25$ K, where $\chi = 0.0135$ emu·mol^{-1}.

The data clearly show an antiferromagnetic coupling between the two picNN free radicals to give an $S = 0$ ground state. An estimate of the radical−radical coupling can thus be derived from the Bleaney−Bowers equation that describes the magnetic behavior of an $S = 1/2$ dimer.[49] The derived value of $J_{\mathrm{rad-rad}}$ (−13.4 cm^{-1}) is about 1 order of magnitude higher than the intermolecular interaction between radicals $j_{\mathrm{rad-rad}}$ observed in most crystalline materials containing free or metal-bonded nitronyl nitroxides, like the manganese(II) complex **7**. This means that $J_{\mathrm{rad-rad}}$ corresponds to a magnetic interaction between radicals that are bonded to the same metal ion. This interaction is stronger because the metal ion brings the two adjacent picNN radicals to a closer distance. In the solid, both $J_{\mathrm{rad-rad}}$ and $j_{\mathrm{rad-rad}}$ interactions are present. This is why a simple dimeric model fails to describe precisely the position of the maximum of the $\chi = f(T)$ curve (see the Supporting Information). We have then used a cluster model that comprises four Zn(picNN)$_2$ units, similar to that described for the manganese(II) compound. The exchange Hamiltonian is thus represented by the second and third terms of eq 3. The best simulation of the magnetic properties was obtained with the following set of exchange coupling parameters: $J_{\mathrm{rad-rad}} = -15$ cm^{-1} and $j_{\mathrm{rad-rad}} = -1.8$ cm^{-1}. The value of $J_{\mathrm{rad-rad}}$ was taken as an estimation of the intramolecular radical−radical interaction in the isostructural complexes **4**, **5**, and **7**.

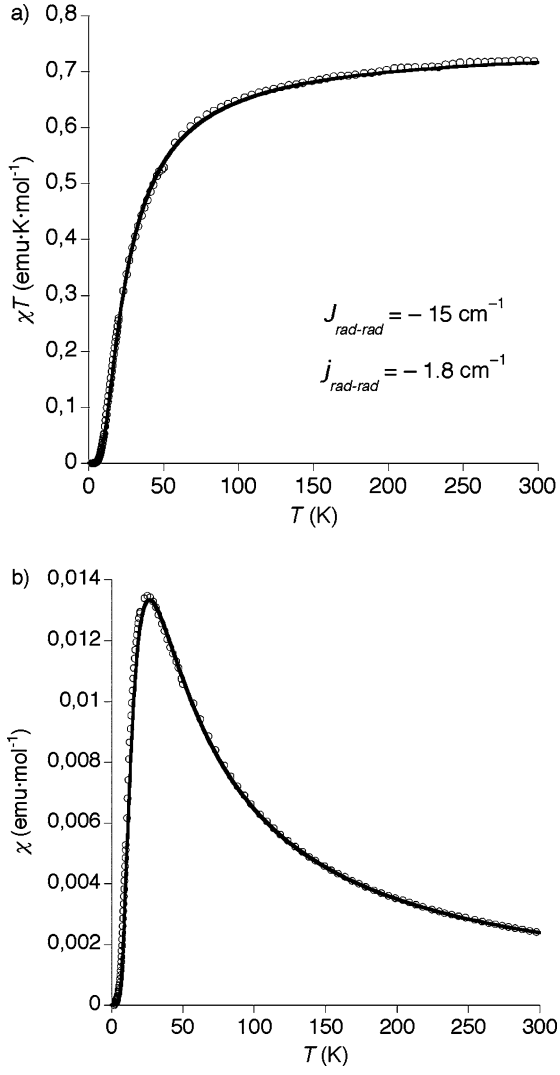

Figure 10. Temperature dependence of χT (a) and χ (b) of **6** (empty circles) and best simulation using the exchange Hamiltonian of eq 3. Inset: Values of the calculated parameters. The exchange interaction pattern is shown in Scheme 2.

[Cu$_4$(picNN)$_4$(H$_2$O)$_4$](ClO$_4$)$_4$·4H$_2$O (8). The χT product at room temperature (0.75 emu·K·mol^{-1}) has a considerably lower value (Figure 11a) than that expected for the presence of eight noninteracting $S = 1/2$ spins (3 emu·K·mol^{-1}) corresponding to four Cu^{2+} ions and four nitroxide radicals per formula unit. Upon cooling, χT decreases smoothly and vanishes at temperatures below 100 K. The thermal variation of the molar magnetic susceptibility χ exhibits (Figure 11b) a similar behavior.

The data are in agreement with the very strong antiferromagnetic coupling between the Cu^{2+} ions and picNN free radicals predicted after the analysis of the structural data. From the magnetic point of view, the compound can be considered as integrated by four equivalent dimeric units of $S = 1/2$ spins that couple antiferromagnetically to give an $S = 0$ ground state. In this case, the remaining interactions present in the system (through-space interactions between nitroxides and copper−copper interactions mediated by the syn−anti carboxylate bridges) are negligible in comparison with the strong copper-nitroxide coupling. The magnetic behavior of **8** can thus be exactly reproduced using the Bleaney−Bowers equation.[49] The exchange Hamiltonian is thus represented by the first term of the first sumatory of eq 3. The derived value of the copper−nitroxide exchange coupling parameter $J_{\mathrm{Cu-rad}} = -268$ cm^{-1} is one of the largest ever reported in this kind of compound.

Discussion

The analysis of the magnetic properties of the isostructural compounds **4**−**7** clearly shows the coexistence of three types of magnetic interactions that differ in the order of magnitude of the exchange coupling parameter J associated with them, namely, (i) a strong metal−radical interaction, on the order

(49) Bleaney, B.; Bowers, K. D. *Proc. R. Soc. London, Ser. A* **1952**, *214*, 451.

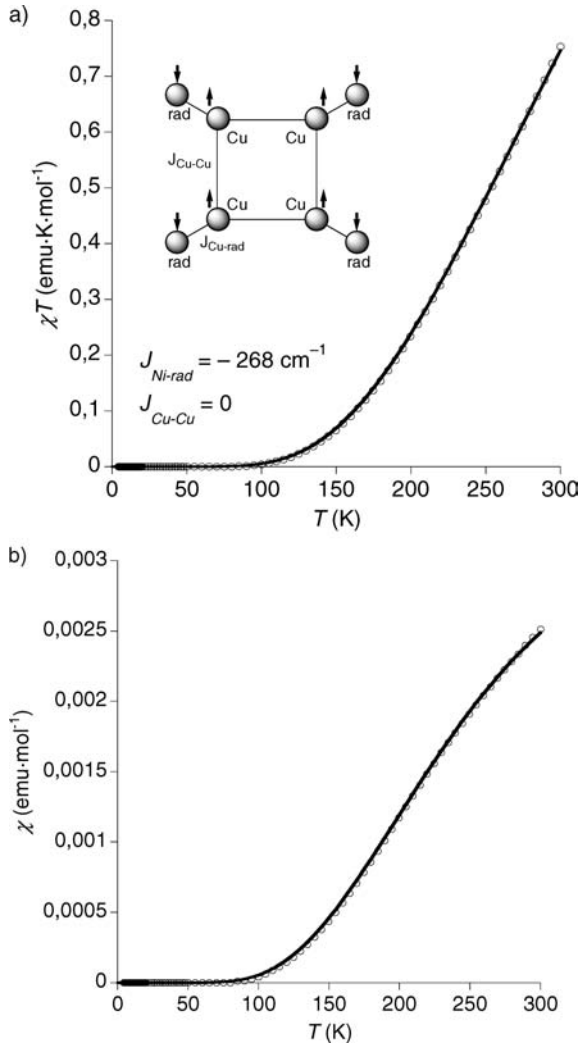

Figure 11. Temperature dependence of χT (a) and χ for **8** (empty circles) and best simulation obtained by applying the Bleaney−Bowers model to four noninteracting dimers of $S = 1/2$ spins.

of 10^2 cm^{-1}, (ii) a moderate interaction (around 10 cm^{-1}) between radicals located in the same metal ion coordination sphere, and (iii) a very weak through-space interaction (around 1 cm^{-1}) between radicals coordinating to different metal centers. Let us examine these interactions in our family of compounds.

The correlation between the magnetic properties and the crystal structure of metal−radical complexes is well understood. The two spin carriers are bound strongly, and the magnetic interaction that results takes place via a direct exchange mechanism. In such a system, the magnetic orbitals are simply the half-occupied orbitals of each spin carrier. The nitronyl nitroxide radical has most of its spin density in a π^* orbital with its axis lying perpendicular to the O−N−C−N−O plane. The metal ions have different magnetic d orbitals given by simple ligand-field theory. According to the Kahn−Briat model, the extent of overlap between magnetic orbitals is responsible for the presence of antiferromagnetic interactions, whereas orthogonality (or symmetry-forbidden overlap) induces ferromagnetic interactions.[50] The magnetic coupling J_{M-rad} actually observed is given by the sum of the two types of contributions.

The nickel(II)−nitroxide compound **4** exhibits global antiferromagnetic behavior with the two nitroxide $S = 1/2$ spins coupled to the Ni^{2+} $S = 1$ spin to give an $S = 0$ ground state. Antiferromagnetic interactions are normally the rule in nickel(II)−nitroxide complexes.[51] Some interesting exceptions appear when the O−N−C−N−O conjugated fragment and the equatorial plane of the complex are coplanar. In this case, the π^* orbital of the radical is orthogonal to the $d_{x^2-y^2}$ metal orbital, while its overlap with the d_{z^2} orbital is symmetry-forbidden.[22] In complex **4**, however, these strict geometrical conditions are not fulfilled. The dihedral angle between its equatorial plane and the O−N−C−N−O nitroxide plane is ca. 75°, very far from coplanarity. As a result, the magnetic interaction between the Ni^{2+} and the free radical is exceptionally strong ($J_{Ni-rad} = -193$ cm^{-1}) as compared to previously reported Ni^{2+}−nitroxide complexes.

In the case of the manganese(II) compound **7**, an antiferromagnetic interaction is expected in any case, irrespective of the geometrical features of the complex. This is due to the high symmetry of the $^6A_1$ metal ground state. The value of the exchange coupling parameter is negative ($J_{Mn-rad} = -98$ cm^{-1}) and higher in magnitude than that in similar compounds. Similar arguments apply to the cobalt(II) complex.

In a second step, we will consider the radical−radical coupling $J_{rad-rad}$ that takes place between the two nitroxide radicals coordinating to the same metal ion. These two radicals sit at very short distances (around 2.8 Å) in compounds **4**−**7**. The $J_{rad-rad}$ interaction is masked in complexes **4**, **5**, and **7**, which exhibit strong metal−radical interactions, but becomes evident in the study of the zinc(II) complex. This interaction has been observed previously and takes place most probably through space. Its value (−15 cm^{-1}) compares well with those previously determined in similar materials.

Finally, the weakest interaction observed in these compounds corresponds to the shortest contacts between free radicals belonging to different coordination spheres. As discussed in the structural section, the pyridine rings of neighboring complexes form stacks due to the presence of $\pi-\pi$ interactions, and this situation brings the corresponding nitroxide functions to a very close distance. As a result, an intermolecular interaction between these radicals, $j_{rad-rad}$ (on the order of 1 cm^{-1}), appears. This interaction becomes apparent in the study of the manganese(II) complex **7** with a well-defined paramagnetic $S = 3/2$ ground state. In **4**−**7**, the very short distance between the free (noncoordinated) N−O functions (O2···O2 around 3.75 Å) and the low value of the dihedral angle between adjacent O−N−C−N−O radical planes (ca. 30°) yields a relatively high value of the intermolecular coupling as compared to similar examples.

The copper(II) compound **8** is particularly interesting due to its cyclic tetrameric structure comprising four nitroxide radicals and four Cu^{2+} ions. In principle, four types of interactions are present in this ring containing eight $S = 1/2$ spins: two metal−radical interactions (Cu1−nitroxide and

(50) Kahn, O.; Briat, B. *J. Chem. Soc., Faraday Trans. 2* **1976**, *72*, 268.

Cu2−nitroxide) and two Cu1−Cu2 interactions mediated by the syn−anti carboxylate bridge. The strong, negative copper−nitroxide interactions are due to the very short copper−nitroxide distances and to the high values of the dihedral angles between the Cu^{2+} equatorial plane ($d_{x^2-y^2}$ orbital) and the O−N−C−N−O fragment (π^* orbital). These values are significantly different for the Cu1−picNN and Cu2−picNN fragments (22° and 33°, respectively), suggesting the presence of two distinct copper−radical interactions. The calculated value of J_{Cu-rad} can then be considered as an average value of the two real coupling constants. It is one of the largest ever reported in the literature for a Cu−NN dimer. Stronger interactions can be sometimes observed for copper complexes of *tert*-butyl nitroxides because the spin density is here concentrated in a single N−O$^{\bullet}$ moiety. Further, chelating *tert*-butyl nitroxides tend to coordinate equatorially in a coplanar arrangement, thus inducing record values of ferromagnetic copper−radical interactions.[4,52]

Similar cyclic tetracopper(II) units containing syn,anti-carboxylate bridges that link equatorial positions of adjacent Cu(II) sites have been reported.[53] In these systems, a weak ferromagnetic Cu−Cu interaction (6−8 cm^{-1}) is generally observed. Even weaker ($|J| < 1$ cm^{-1}, J can be positive or negative) is the interaction between two Cu^{2+} ions linked by a syn,anti-carboxylate bridge in an equatorial−axial mode. Clearly, these two interactions cannot be detected in **8**, which is diamagnetic at temperatures below 100 K.

(51) Caneschi, A.; Gatteschi, D.; Renard, J. P.; Rey, P.; Sessoli, R. *Inorg. Chem.* **1989**, *28*, 2940–2944.
(52) Osanai, K.; Okazawa, A.; Nogami, T.; Ishida, T. *J. Am. Chem. Soc.* **2006**, *128*, 14008–14009.
(53) Murugesu, M.; Clérac, R.; Pilawa, B.; Mandel, A.; Anson, C. E.; Powell, A. K. *Inorg. Chim. Acta* **2002**, *337*, 328–336.

Conclusion

A terdentate nitronyl nitroxide free radical derived from the picolinate anion (picNN) forms stable neutral complexes of 1:2 metal-to-ligand stoichiometry with different first-row transition metal ions. Extremely large antiferromagnetic metal−nitroxide interactions have been observed. These interactions can be clearly correlated to the structure of the different complexes. Further work will be directed to the study of neutral lanthanide−radical complexes that can exhibit interesting electroluminescent properties.

Complexation with copper(II) affords a cyclic structure containing four carboxylate-bridged Cu^{2+} ions and four radical units. The copper(II)−nitroxide exchange interaction is one of the largest ever reported in the literature. This compound demonstrates that it is possible to build heterospin extended systems by incorporating potentially bridging ligands in the structure of a chelating radical.

Acknowledgment. We thank José M. Martínez-Agudo for the magnetic measurements and Dr. Clemente-Juan for helpful discussions. We acknowledge financial support from the European Union (NoE Magmanet), the Ministerio de Educación y Ciencia (Projects MAT2004-03849, MAT2007-61584, and CONSOLIDER-INGENIO in Molecular Nanoscience), and Generalitat Valenciana.

Supporting Information Available: Figure S1, giving a $\chi = f(T)$ plot for **6**, together with the best fit to the Bleaney−Bowers equation. Complete crystal structure details are given in CIF format. This material is available free of charge via the Internet at http://pubs.acs.org.

IC802218J